PAPER • OPEN ACCESS

Traveling concentration pulses of bacteria in a generalized Keller–Segel model

To cite this article: Maximilian Seyrich *et al* 2019 *New J. Phys.* **21** 103001

New Journal of Physics
The open access journal at the forefront of physics

Deutsche Physikalische Gesellschaft DPG
IOP Institute of Physics

Published in partnership with: Deutsche Physikalische Gesellschaft and the Institute of Physics

OPEN ACCESS

RECEIVED
25 April 2019

REVISED
22 August 2019

ACCEPTED FOR PUBLICATION
17 September 2019

PUBLISHED
1 October 2019

PAPER

Traveling concentration pulses of bacteria in a generalized Keller–Segel model

Maximilian Seyrich[1], **Andrzej Palugniok**[1,2] **and Holger Stark**[1,3]

[1] Institut für Theoretische Physik, Technische Universität Berlin, Hardenbergstrasse 36, D-10623 Berlin, Germany
[2] Worcester College, University of Oxford, Walton Street, OX1 2HB Oxford, United Kingdom
[3] Author to whom any correspondence should be addressed.

E-mail: seyrich@tu-berlin.de, andrzej.palugniok@worc.ox.ac.uk and holger.stark@tu-berlin.de

Keywords: Keller–Segel model, *E.coli*, maximum carrying capacity, collective active matter, bacterial pulse

Supplementary material for this article is available online

Abstract

We formulate a Markovian response theory for the tumble rate of a bacterium moving in a chemical field and use it in the Smoluchowski equation. Based on a multipole expansion for the one-particle distribution function and a reaction-diffusion equation for the chemoattractant field, we derive a polarization extended model, which also includes the recently discovered angle bias. In the adiabatic limit we recover a generalized Keller–Segel equation with diffusion and chemotactic coefficients that depend on the microscopic swimming parameters. Requiring the tumble rate to be positive, our model introduces an upper bound for the chemotactic drift velocity, which is no longer singular as in the original Keller–Segel model. Solving the Keller–Segel equations numerically, we identify traveling bacterial concentration pulses, for which we do not need a second, signaling chemical field nor a singular chemotactic drift velocity as demanded in earlier publications. We present an extensive study of the traveling pulses and demonstrate how their speeds, widths, and heights depend on the microscopic parameters. Most importantly, we discover a maximum number of bacteria that the pulse can sustain—the maximum carrying capacity. Finally, by tuning our parameters, we are able to match the experimental realization of the traveling bacterial pulse.

1. Introduction

Collective motion of biological and artificial microswimmers shows a broad range of interesting phenomena as demonstrated in several review articles [1–5]. The formation of various patterns and clustering have been investigated both experimentally and theoretically in systems of bacteria [6–13], of eukaryotic cells such as *Dictyostelium discoideum* or human sperm [14–22], as well as in suspensions of active colloids [4, 23–32]. In this article we study the collective behavior of a bacterial population, which in the concentration field of a chemoattractant forms a traveling solitary pulse.

The motility mechanism of the run-and-tumble bacterium *E.coli* has been extensively studied [33–40]. Bacteria perform chemotaxis, the ability to sense and respond to chemical gradients in order to find better living conditions. They realize the chemotactic drift motion along a chemical gradient by elongated run phases if the environment becomes more favorable while runs are shortened in the opposite case [39–41]. The internal chemotaxis machinery of the bacterium senses and compares the nutrient concentration in time, which is rationalized in a linear response theory for the tumble rate [34, 42–44]. More recently, a second chemotaxis strategy, called angle bias, has been reported [36, 39, 40]. The mean reorientation angle during tumbling is reduced if the bacterium swims along a chemical gradient and increased in the opposite case. This also generates a net drift motion in the favorable direction. Finally, using logarithmic sensing, *E.coli* is able to perform chemotaxis in concentration fields varying by many orders of magnitude [45–47]. Such an ability is commonly described by Weber's law in different physical areas [48, 49].

A very interesting collective phenomenon in a bacterial population is a concentration pulse that travels along a capillary tube with almost no dispersion nearly like a soliton [6, 36], most recently also observed in a population with non-genetic variations [50]. The pulse is initiated in an initially uniform environment of a chemoattractant. A bacterial population concentrated in space eats the nutrient and thereby creates a chemical gradient along which it drifts towards untouched regions. Moreover, Adler in his experiments also observed that not all bacteria travel with the pulse but are left behind at the initial location [6], which indicates a finite carrying capacity of the traveling pulse. Further chemoattractants present in Adler's experiments then initiated further pulses emerging from the bacteria left behind.

A very prominent theoretical approach to describe the traveling bacterial pulse is the celebrated Keller–Segel model [51], originally introduced for the aggregation of slime molds [52]. It couples a diffusion-drift equation for the bacterial density to a reaction equation for the nutrient. However, the Keller–Segel model has two drawbacks. First, a soliton solution (classified as unstable [53]) only occurs if the chemotactic drift velocity diverges for vanishing nutrient concentration. Second, nutrient diffusion was neglected. Later, based on analytic arguments, [53] demonstrated that traveling pulses also exist in the presence of nutrient diffusion. More importantly, Brenner *et al.* showed that the singularity in the chemotactic drift velocity is not necessary if one introduces a second chemoattractant, which the bacteria excrete themselves [54]. Reference [36] followed this approach to formulate a kinetic model (inspired by [55]), which describes traveling pulses in their experiments. Finally, a modification of this kinetic model has recently been used to investigate pulse propagation in the presence of two *E.coli* populations [56]. The Keller–Segel equations find wide applications in modeling bacterial chemotaxis as reviewed in [57]. They have also been derived for active Brownian particles, which propel by self-diffusiophoresis, and for quorum-sensing run-and-tumble particles [58].

Multipole expansions have frequently been applied to microswimmers in order to approximate the Smoluchowski equation for the full distribution function in the microswimmer's position and orientation [13, 27, 58–60]. Besides for density such expansions also provide an additional dynamic equation for the polarization, which unraveled interesting collective behavior of Janus particles [29] and which also allowed to investigate steady-state distributions of run-and tumble particles [61]. Our derivation is inspired by the approach of the latter reference but extends it by introducing the concentration field of a chemoattractant.

In this article we formulate a Markovian response theory for the tumble rate. It includes logarithmic sensing for which we introduce an upper threshold. We use the tumble rate in the Smoluchowski equation and derive a polarization extended model (PE) to treat chemotaxis of non-interacting *E.coli* bacteria. The PE model contains equations for the bacterial density, the bacterial polarization, and the chemical concentration field. In a second step, we also include the recently discovered angle bias. In the adiabatic limit the PE model simplifies to a generalized Keller–Segel model (KS) where the coefficients for diffusion and chemotactic drift velocity depend on the microscopic swimming parameters of the bacterium. In particular, the chemotactic coefficient is not singular in the chemical concentration. We numerically solve both models for an initially uniform chemoattractant and a bacterial population concentrated in space using parameters that are realistic for the *E.coli* bacterium. The traveling bacterial pulse generated by both the PE and KS model are identical thus the KS model is a valid approximation of the full kinetic formalism. We present a detailed parameter study of the traveling pulse and identify a maximum carrying capacity as a consequence of the bounded chemotactic drift velocity, which has not been mentioned so far. It means that the pulse can only sustain a finite number of bacteria. Finally, we tune our parameters to match the experimental realization of the bacterial pulse in [36]. Hence, our generalized Keller–Segel model is able to describe traveling bacterial pulses without the need neither for a singular chemotactic drift velocity nor for a second chemoattractant.

The remainder of the article is organized as follows. We present the Markovian response theory for the tumble rate in section 2.1. We use it to derive the polarization extended model (PE) and the generalized Keller–Segel model (KS) in sections 2.2 and 2.3. We also incorporate the angle bias and formulate a non-dimensional version of the KS model in sections 2.4 and 2.5. Details of the numerical solution scheme are given in sections 3 and 4 presents our detailed numerical study. We close with conclusions and an outlook in section 5.

2. Model

2.1. Markovian response theory for tumble rate

Bacteria tumble less when moving up a chemical gradient. Based on the established linear-response theory, we formulate an equation for the tumble rate $\lambda(\mathbf{r}, \mathbf{e})$ as a function of the swimming direction $\mathbf{e}$. Below, we will relate it to the angle θ relative to the local gradient ∇c of a chemoattractant with density c.

We start with the linear-response theory [43]. It gives the tumble rate $\lambda(t)$ as a function of time and depends on the bacterium's past trajectory $\mathbf{r}(t')$

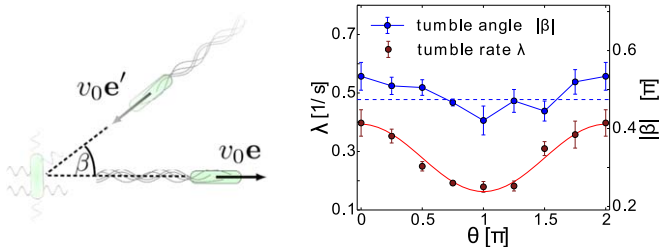

Figure 1. Left: schematic of an individual *E.coli* tumbling from its previous direction $\mathbf{e}'$ to $\mathbf{e}$ with tumble angle β. Right: mean tumble rate $\lambda(\theta)$ (red) as a function of the swimming angle θ measured against the negative chemical gradient. The tumble rate was averaged over a population of around 1.000 *E.coli* in a linear gradient of α-methyl-aspartate. The fit with a cosine function, $y(x) = a_1 + a_2\cos(x)$ (red line) according to equation (2), yields regression parameters $a_1 = 0.278$ and $a_2 = 0.115$. The blue line represents the mean tumble angle $\langle \cos\beta\rangle(\theta)$ as a function of θ of the same population. It indicates an angle bias for tumbling in a chemical gradient. Adapted from [39].

$$\lambda(t) = \lambda_{\mathrm{equ}} - \int_{-\infty}^{t} R(t-t')\, c(\mathbf{r}(t'))\mathrm{d}t', \tag{1}$$

where we have introduced the response kernel $R(t)$ and λ_{equ} is the tumble rate without any chemical gradient. Note that equation (1) describes a non-Markovian process. In appendix A we convert it to a Markovian process with λ depending on location $\mathbf{r}$ and swimming direction $\mathbf{e}$ by averaging over all possible bacterial trajectories in order to obtain the mean history for a given swimming direction $\mathbf{e}$. Thus, the tumble rate we give below is an averaged quantity suitable to be used in a continuum theory. To derive it, we split the integral on the rhs of equation (1) into contributions from individual runs, during which the according swimming directions $\mathbf{e}_i$ are assumed to be constant. Averaging over the history of all possible paths, we can show that each of these contributions gives a term proportional to the scalar product $\mathbf{e}\cdot\frac{\nabla c}{c}$. The factor $1/c$ results from the fact that the response kernel is proportional to the inverse background concentration, $R\propto 1/c$, which was indeed measured in experiments for the chemoattractant alpha-methyl-aspartate in [38]. This chemoattractant is widely used, e.g. in the seminal experiments of [33, 34, 38, 62] and also in experiments of [39, 40]. For the detailed derivation we refer to appendix A and present the final result

$$\lambda(\mathbf{r},\,\mathbf{e}) = \lambda_{\mathrm{equ}} - \chi_0 v_0 \mathbf{e}\cdot\frac{\nabla c(\mathbf{r})}{c(\mathbf{r})}. \tag{2}$$

Here, v_0 is the swimming velocity of the bacterium and χ_0 is a unitless measure of the chemotactic strength. It depends on integrals over the response function R and moments of the tumble angle distribution $P(\beta)$. Note that we obtain here $\lambda\propto\nabla(\ln c)$ commonly known as logarithmic sensing and Weber's law. It was measured, for example, in [47]. The linear dependence of the tumble rate λ on $\nabla c(\mathbf{r})\cdot\mathbf{e}$ was already introduced by Schnitzer as the leading order for the angular variation of λ [61]. It follows directly from equation (1) by choosing $R(t-t')$ proportional to the time derivative of the δ function as demonstrated by Locsei in [63]. This article also calculates the chemotactic drift speed (see section 2.3) by performing an average over all possible bacterial trajectories similar to our approach. Indeed, in appendix A we show that we arrive at the same chemotactic drift speed for the specific response function chosen in [63].

When we define the orientation angle relative to the negative chemical gradient, $\cos\theta = -\mathbf{e}\cdot\frac{\nabla c}{|\nabla c|}$, the tumble rate becomes

$$\lambda(\mathbf{r},\,\theta) = \lambda_{\mathrm{equ}} + \chi_0 v_0 \frac{|\nabla c(\mathbf{r})|}{c(\mathbf{r})}\cos\theta. \tag{3}$$

In figure 1 adapted from [39], the red points show experimental data for the mean tumble rate $\lambda(\mathbf{r},\,\theta)$. It was obtained by averaging over a population of around 1000 individual bacteria in a linear gradient. The appropriate cosine fit (red line) confirms our theoretically derived result of equation (2) and was the motivation to derive it from the linear-response theory.

A biologically relevant tumble rate should have both a sensing threshold [64] as well as a saturation of the response to the chemoattractant [65], which is not present in equation (2). First, it is known that the bacterium needs a small threshold concentration c_t to perform chemotaxis since it senses the chemical field by chemoreceptors [64]. Second, equation (2) produces a negative tumble rate for a sufficiently large gradient of $\log c$, which is even singular at $c = 0$. In our derivation the singularity arises from the relation $R\propto 1/c$ for the response function mentioned earlier. While $R\propto 1/c$ was measured for a wide range of background concentrations [38], clearly the second term on the right-hand side of equation (2) has to saturate to a value smaller than λ_{equ} to keep the tumble rate positive. There a several approaches to remedy these shortcomings. The threshold concentration was implemented, e.g. in [51, 66, 67] by shifting the singularity in equation (2) from

$c = 0$ to c_t. To implement a saturation in the chemotactic response, [67, 68] among others used the so-called receptor law, while [36, 69] introduced a hyperbolic tangent function. To implement both the sensing threshold and the saturation in the chemotactic response, we decided to use the hyperbolic tangent function in equation (2) and write

$$\lambda(\mathbf{r}, \mathbf{e}) = \lambda_{\mathrm{equ}} - \chi\left(\frac{|\nabla c|}{c}\right)\mathbf{e}\cdot\hat{\mathbf{s}} \tag{4}$$

with

$$\chi\left(\frac{|\nabla c|}{c}\right) := \chi_0 \frac{v_0}{\delta}\tanh\left(\frac{c}{c_t}\right)\tanh\left(\delta\frac{|\nabla c|}{c}\right). \tag{5}$$

Here, we have introduced $\hat{\mathbf{s}} = \frac{\nabla c}{|\nabla c|}$ and do not explicitly state the space dependence of the concentration c. This expression recovers equation (2) for $\delta|\nabla c|/c < 1$ and $c > c_t$, while it smoothly approaches the minimum tumble rate $\lambda_{\mathrm{equ}} - \chi_0\frac{v_0}{\delta}$ for $\delta|\nabla c|/c > 1$ (saturation in the chemotactic response) or it tends to λ_{equ} for $c < c_t$ (sensing threshold). The chemotactic length δ quantifies the strength of the logarithmic derivative of $c(\mathbf{r})$. Appendix B presents a parameter study for the tumble rate of equation (4). Finally, we note that in this article the swimming speed v_0 is constant. If it varies, one always has to make sure that $\chi_0 v_0/\delta < \lambda_{\mathrm{equ}}$ to keep the tumble rate positive.

2.2. Polarization extended model (PE)

2.2.1. Smoluchowski equation

We first construct dynamic equations for the evolution of the one-particle distribution function $\psi(\mathbf{r}, \mathbf{e}, t)$ of position $\mathbf{r}$ and orientation $\mathbf{e}$ at time t and the concentration of chemoattractant, $c(\mathbf{r}, t)$. We begin with a generalized Smoluchowski equation for ψ [55, 61, 70–72], which contains the usual contributions from translational and rotational currents, $\mathbf{J}_{\mathrm{trans}}$ and $\mathbf{J}_{\mathrm{rot}}$, but also contributions from tumble events represented by $\mathcal{F}\{\psi\}$ and from cell division and death, $\frac{\alpha}{S_d}\int\psi(\mathbf{r}, \mathbf{e}', t)\mathrm{d}\mathbf{e}'$:

$$\frac{\partial\psi}{\partial t} = -\nabla\cdot\mathbf{J}_{\mathrm{trans}} - R\cdot\mathbf{J}_{\mathrm{rot}} + F\{\psi\} + \frac{\alpha}{S_d}\int\psi(\mathbf{r}, \mathbf{e}', t)\mathrm{d}\mathbf{e}'. \tag{6}$$

Here, $\mathcal{R} = \mathbf{e}\times\partial_{\mathbf{e}}$ where $\partial_{\mathbf{e}} = (\partial_{e_x}, \partial_{e_y}, \partial_{e_z})$ denotes the nabla operator in orientation space and $\alpha = \ln(2)/\tau$ is the net growth rate with τ being the mean doubling time of bacterial cells [36]. We also assume that the net growth of cells does not depend of their directon $\mathbf{e}$ and S_d is the surface area of a d dimensional unit sphere (full solid angle). For the translational current we include active motion and translational diffusion, $\mathbf{J}_{\mathrm{trans}} = v_0\mathbf{e}\psi - D\nabla\psi$, where D is the translational diffusion coefficient and v_0 is the bacterial swimming speed. The rotational current is purely diffusive, $\mathbf{J}_{\mathrm{rot}} = -D_{\mathrm{rot}}\mathcal{R}\psi$, where D_{rot} is the rotational diffusion coefficient. According to [33] we take a Poisson distribution for the run times and write the term for the tumble events as

$$\mathcal{F}\{\psi\} = -\lambda(\mathbf{r}, \mathbf{e})\psi + \int P(\mathbf{e} - \mathbf{e}', \mathbf{e}')\lambda(\mathbf{r}, \mathbf{e}')\psi(\mathbf{r}, \mathbf{e}', t)\mathrm{d}\mathbf{e}'. \tag{7}$$

We introduced the tumble rate $\lambda(\mathbf{r}, \mathbf{e})$ and $P(\mathbf{e} - \mathbf{e}', \mathbf{e}')$ is the probability of a bacterium to reorient from orientation $\mathbf{e}'$ to $\mathbf{e}$. In equation (7) the first term on the rhs represents events, which cause bacteria with orientation $\mathbf{e}$ to tumble into any orientation, and the second term represents all events, which cause bacteria with other orientations to tumble into orientation $\mathbf{e}$. The complete Smoluchowski equation for the evolution of ψ now reads

$$\begin{aligned}\frac{\partial\psi}{\partial t} &= -\nabla\cdot(v_0\mathbf{e}\psi) + D\nabla^2\psi + D_{\mathrm{rot}}R^2\psi - \lambda(\mathbf{r}, \mathbf{e})\psi + \int P(\mathbf{e} - \mathbf{e}', \mathbf{e}')\lambda(\mathbf{r}, \mathbf{e}')\psi(\mathbf{r}, \mathbf{e}', t)\mathrm{d}\mathbf{e}' \\ &\quad + \frac{\alpha}{S_d}\int\psi(\mathbf{r}, \mathbf{e}', t)\mathrm{d}\mathbf{e}'.\end{aligned} \tag{8}$$

For completeness, we write a reaction-diffusion equation for the chemoattractant concentration c, which is also consumed by bacteria with constant rate k

$$\frac{\partial c}{\partial t} = D_c\nabla^2 c - k\int\psi(\mathbf{r}, \mathbf{e}', t)\mathrm{d}\mathbf{e}'. \tag{9}$$

2.2.2. Multipole expansion

In order to proceed with equations (8) and (9), we assume that the probability distribution for a specific tumble event does not depend on the initial orientation of the bacterium, $P(\mathbf{e} - \mathbf{e}', \mathbf{e}') = P(\mathbf{e} - \mathbf{e}')$. Therefore, we can write for the zeroth and first moment

$$\int P(\mathbf{e}-\mathbf{e}')\mathrm{d}\mathbf{e}=1, \tag{10}$$

$$\int \mathbf{e}P(\mathbf{e}-\mathbf{e}')\mathrm{d}\mathbf{e}=\langle\cos\beta\rangle\mathbf{e}', \tag{11}$$

where $\langle\cos\beta\rangle$ is the mean of the cosine of the reorientation angle β [61]. We take the tumble rate $\lambda(\mathbf{r},\mathbf{e})$ to vary as in equation (4). Now, we integrate equation (8) over all orientations $\mathbf{e}$ and define the bacterial density $\rho(\mathbf{r},t)=\int\psi(\mathbf{r},\mathbf{e},t)\mathrm{d}\mathbf{e}$ and polarization $\mathbf{P}(\mathbf{r},t)=\int\mathbf{e}\psi(\mathbf{r},\mathbf{e},t)\mathrm{d}\mathbf{e}$, which correspond to the zeroth and first moments of ψ, respectively, and obtain [61, 73]

$$\frac{\partial\rho}{\partial t}=-\boldsymbol{\nabla}\cdot(v_0\mathbf{P})+D\nabla^2\rho+\alpha\rho. \tag{12}$$

We have also used $\int\mathcal{R}^2\psi\mathrm{d}\mathbf{e}=0$ and the normalization condition equation (10) to show that tumbling does not contribute to equation (12).

In order to derive a dynamic equation for the polarization, we compute $\int\mathbf{e}$ equation (8) $\mathrm{d}\mathbf{e}$ and introduce the quadrupole moment $\mathbf{Q}=\int(\mathbf{e}\otimes\mathbf{e}-\frac{1}{d})\psi(\mathbf{r},\mathbf{e},t)\mathrm{d}\mathbf{e}$ with d being the number of spatial dimensions. This gives

$$\begin{aligned}\frac{\partial\mathbf{P}}{\partial t}=&-v_0\boldsymbol{\nabla}\mathbf{Q}-\frac{v_0}{d}\boldsymbol{\nabla}\rho+D\nabla^2\mathbf{P}-[D_{\mathrm{rot}}(d-1)+(1-\langle\cos\beta\rangle)\lambda_{\mathrm{equ}}]\mathbf{P}\\&+(1-\langle\cos\beta\rangle)\chi\left(\frac{|\boldsymbol{\nabla}c|}{c}\right)\mathbf{Q}\hat{\mathbf{s}}+\frac{1-\langle\cos\beta\rangle}{d}\chi\left(\frac{|\boldsymbol{\nabla}c|}{c}\right)\rho\,\hat{\mathbf{s}},\end{aligned} \tag{13}$$

where we used $\mathcal{R}^2\mathbf{e}=-(d-1)\mathbf{e}$ and equation (11). To truncate the multipole expansion, we neglect the quadrupole moment $\mathbf{Q}$, which strictly means that the orientational distribution hardly deviates from the isotropic distribution and the deviation can be well described by the polarization. We also define the relaxation rate

$$\omega=D_{\mathrm{rot}}(d-1)+(1-\langle\cos\beta\rangle)\lambda_{\mathrm{equ}}, \tag{14}$$

with which polar order relaxes or decorrelates in time. Thus, we ultimately obtain

$$\frac{\partial\mathbf{P}}{\partial t}=-\omega\mathbf{P}+D\nabla^2\mathbf{P}-\frac{v_0}{d}\boldsymbol{\nabla}\rho+\frac{1-\langle\cos\beta\rangle}{d}\chi\left(\frac{|\boldsymbol{\nabla}c|}{c}\right)\rho\,\hat{\mathbf{s}}. \tag{15}$$

Finally, with our definition of bacterial density ρ we can write equation (9) in a simpler form

$$\frac{\partial c}{\partial t}=D_c\nabla^2c-k\rho. \tag{16}$$

2.3. The Keller–Segel model as adiabatic limit

In the case of high Peclet numbers ($Pe=av_0/D\gg1$), where we can neglect translational diffusion[4], and on large times $t\gg\frac{1}{\omega}$, where the adiabatic limit $\frac{\partial\mathbf{P}}{\partial t}\approx0$ applies, the polarization from equation (15) becomes

$$\mathbf{P}=-\frac{v_0}{\omega d}\boldsymbol{\nabla}\rho+\frac{1-\langle\cos\beta\rangle}{\omega d}\chi\left(\frac{|\boldsymbol{\nabla}c|}{c}\right)\rho\,\hat{\mathbf{s}}. \tag{17}$$

We remind that $\hat{\mathbf{s}}=\boldsymbol{\nabla}c/|\boldsymbol{\nabla}c|$. Substituting equation (17) into (12), we obtain the generalized Keller–Segel model

$$\frac{\partial\rho}{\partial t}=D_{\mathrm{eff}}\nabla^2\rho+\alpha\rho-\frac{v_0(1-\langle\cos\beta\rangle)}{\omega d}\boldsymbol{\nabla}\cdot\left[\chi\left(\frac{|\boldsymbol{\nabla}c|}{c}\right)\rho\,\hat{\mathbf{s}}\right], \tag{18}$$

$$\frac{\partial c}{\partial t}=D_c\nabla^2c-k\rho, \tag{19}$$

where $D_{\mathrm{eff}}=v_0^2/\omega d+D\approx v_0^2/\omega d$ is the typical translational diffusion coefficient of an active particle, the orientation of which decorrelates on the characteristic time ω^{-1}. The approximate expression for D_{eff} is valid at high Peclet numbers.

From the third term on the rhs of equation (18) we read off the chemotactic velocity along the chemical gradient

$$\mathbf{v}_{\mathrm{ch}}=\frac{v_0(1-\langle\cos\beta\rangle)}{\omega d}\chi\left(\frac{|\boldsymbol{\nabla}c|}{c}\right)\hat{\mathbf{s}}. \tag{20}$$

[4] Note, in addition, keeping the diffusion term in the polarization equation (17) would generate spatial derivatives larger than two in equation (18), which we neglect here. This can be seen, when looking at the spatial Fourier transform in k space.

Taking $\chi = \chi_0 v_0 |\nabla c|/c$, we recover the model suggested by Keller and Segel with $\mathbf{v}_{ch} \propto \nabla c/c$ [51], and the chemotactic drift velocity is determined by a combination of microscopic parameters, $\frac{\chi_0 v_0^2 (1 - \langle \cos\beta \rangle)}{\omega d}$, called the chemotactic constant. However, as stated earlier, according to equation (2) the original form for χ implies negative tumble rates for small c and sufficiently steep chemoattractant gradient. The maximum value that χ can physically assume is λ_{equ}, where the tumble rate becomes negative. As a result, the chemotactic speed $v_{ch} = |\mathbf{v}_{ch}|$ is also bounded. Taking $\chi = \lambda_{equ}$ and approximating $\omega \approx (1 - \langle \cos\beta \rangle)\lambda_{equ}$ since D_{rot} in equation (14) is usually much smaller than λ_{equ}, we find

$$v_{ch} \leqslant \frac{v_0}{d}. \tag{21}$$

This shows that an appropriately bounded tumble rate is closely linked to a physically bounded chemotactic drift speed. Furthermore, in appendix C we will show that this upper bound implies an upper bound for the speed of the traveling bacterial pulse and thereby for the maximum number of bacteria it can carry. We will address this point in section 4.

2.4. Bias of tumble angles

Up to this point we have ignored the effect of a bias in the tumble angle towards smaller mean values when swimming up the chemical gradient. This has recently been observed in experiments [36, 39]. We now introduce it by allowing the probability distribution for a specific tumble event to explicitly depend on the initial orientation of the bacterium, $\mathbf{e}'$. Hence equations (10) and (11) become

$$\int P(\mathbf{e} - \mathbf{e}', \mathbf{e}')\mathrm{d}\mathbf{e} = 1, \tag{22}$$

$$\int \mathbf{e} P(\mathbf{e} - \mathbf{e}', \mathbf{e}')\mathrm{d}\mathbf{e} = \langle \cos\beta \rangle (\mathbf{e}')\, \mathbf{e}'. \tag{23}$$

Equation (22) states that the distribution is always normalized irrespective of the initial orientation of the bacterium. In equation (23) the value of the mean cosine of the tumble angle $\langle \cos\beta \rangle (\mathbf{e}')$ now explicitly depends on the initial orientation $\mathbf{e}'$ before the tumble event.

The effect of an angle bias is to lower the mean tumble angle when the bacterium aligns with the chemoattractant gradient, hence the value of $\langle \cos\beta \rangle (\mathbf{e}')$ will increase for stronger alignment. Expanding $\langle \cos\beta \rangle (\mathbf{e}')$ up to the first Legendre polynomial, thus taking into account the leading polar correction, yields

$$\langle \cos\beta \rangle (\mathbf{e}') = \langle \cos\beta \rangle_0 + \sigma\left(\frac{|\nabla c|}{c}\right)\mathbf{e}' \cdot \hat{\mathbf{s}}, \tag{24}$$

where σ is a positive and monotonically increasing function. It is bounded such that its maximum value $\sigma_{max} \leqslant 1 - \langle \cos\beta \rangle_0$, with $\langle \cos\beta \rangle_0$ being the mean cosine of the tumble angle, when the angle bias is not taken into account. Using equations (2), (22)–(24), we can retrace the steps of the multipole expansion (see appendix D for details) to obtain an extended form for equation (15) with equations (12) and (16) remaining unchanged

$$\begin{aligned}\frac{\partial \mathbf{P}}{\partial t} = &-\left\{\omega 1 + \left[\frac{1}{d+2}\chi\left(\frac{|\nabla c|}{c}\right)\sigma\left(\frac{|\nabla c|}{c}\right)\right](1 + 2\hat{\mathbf{s}} \otimes \hat{\mathbf{s}})\right\}\mathbf{P} + D\nabla^2\mathbf{P} - \frac{v_0}{d}\nabla\rho \\ &+ \left[\frac{1 - \langle\cos\beta\rangle_0}{d}\chi\left(\frac{|\nabla c|}{c}\right) + \frac{\lambda_{equ}}{d}\sigma\left(\frac{|\nabla c|}{c}\right)\right]\rho\, \hat{\mathbf{s}}.\end{aligned} \tag{25}$$

Here, $\otimes$ means dyadic product and $(1 + 2\hat{\mathbf{s}} \otimes \hat{\mathbf{s}})\mathbf{P} = \mathbf{P} + 2\hat{\mathbf{s}}\, \hat{\mathbf{s}} \cdot \mathbf{P}$, where $\cdot$ means scalar product.

One immediately recognizes that the angle bias renormalizes the relaxation rate of the polarization and makes it anisotropic. Thus polarizations along and perpendicular to the chemical gradient relax with different rates. In the adiabatic limit $\frac{\partial \mathbf{P}}{\partial t} \approx 0$ and for large Pe we can again solve for the polarization by inverting the matrix in front of $\mathbf{P}$ in equation (25). Substituting the resulting equation into equation (12), we again obtain a generalized Keller–Segel equation and a chemotactic velocity $\mathbf{v}_{ch}$ along the chemical gradient. It now also depends on the angle bias quantified by σ. We refrain from giving the lengthy expression.

2.5. Rescaling the Keller–Segel equations

In order to identify essential parameters especially in the generalized Keller–Segel equations (18) and (19), we introduce unitless quantities. First, we rescale time with the chemical consumption rate, $\tilde{t} = kt$, lengths by the distance $l = \left(\frac{v_0^2}{\omega d k}\right)^{1/2}$, by which a bacterium diffuses in time k^{-1}, thus $\tilde{\mathbf{r}} = \mathbf{r}/l$, and the net growth rate by k, $\tilde{\alpha} = \alpha/k$. Second, we refer the bacterial and chemical densities to their initial values, $\tilde{\rho} = \rho/\rho_0$ and $\tilde{c} = c/c_0$, respectively. Finally, we introduce the rescaled chemotactic length $\tilde{\delta} = \delta/l$ and the rescaled threshold density $\tilde{c}_t = c_t/c_0$. This allows us to write the generalized Keller–Segel equations (18) and (19), where chemotactic response is bounded by the hyperbolic tangents, in rescaled form:

$$\frac{\partial\tilde{\rho}}{\partial\tilde{t}} = \tilde{\nabla}^2\tilde{\rho} + \tilde{\alpha}\tilde{\rho} - \chi_0(1 - \langle\cos\beta\rangle)/\tilde{\delta}\,\tilde{\boldsymbol{\nabla}}\cdot\left[\tanh\left(\frac{\tilde{c}}{\tilde{c}_t}\right)\tanh\left(\tilde{\delta}\frac{|\tilde{\boldsymbol{\nabla}}\tilde{c}|}{\tilde{c}}\right)\tilde{\rho}\;\hat{\mathbf{s}}\right] \tag{26}$$

$$\frac{\partial\tilde{c}}{\partial\tilde{t}} = \frac{D_c}{D_{\text{eff}}}\tilde{\nabla}^2\tilde{c} - \frac{\rho_0}{c_0}\tilde{\rho}. \tag{27}$$

To arrive at this form, we used $D_{\text{eff}} \approx v_0^2/\omega d$, where we neglected the thermal contribution to D_{eff}. We recognize that the rescaled Keller–Segel equations are described by a set of six relevant parameters: $\left\{\frac{D_c}{D_{\text{eff}}},\ \tilde{\alpha},\ \chi_0(1 - \langle\cos\beta\rangle),\ \frac{\rho_0}{c_0},\ \tilde{\delta},\ \tilde{c}_t\right\}$.

3. Details of numerical solution scheme

In the following we study in detail traveling bacterial pulses in an initally uniform density field of a chemoattractant by numerically solving both the polarization extended model (PE) of equations (12), (15) and (16) and the generalized Keller–Segel model (KS) of equations (18) and (19). The experiments in [36] are performed in microchannels with cross section A. Neglecting any influence from the channel walls, we take the three-dimensional system ($d = 3$) to be quasi infinitely extended perpendicular to the channel axis. Thus all densities just depend on the x coordinate along the channel and by symmetry only the x component of the polarization is non-zero.

To solve the respective system of equations, we apply a predictor-corrector method at any given time step to efficiently propagate the field variables in time [74]. As initial field values we choose an exponentially distributed bacterial density, $\rho(x,\ t = 0) = \rho_0\exp(-x/x_0)$, a uniform density of the chemoattractant, $c(x, t = 0) = c_0$, and zero polarization $P_x(x, t = 0) = 0$. During time integration no-flux boundary conditions are employed at $x = 0$ and at sufficiently large x_∞, such that

$$\partial_x\rho|_{0,x_\infty} = 0 \quad \text{and} \quad \partial_x c|_{0,x_\infty} = 0 \tag{28}$$

while we assume that polarization stays zero, $P_x|_{0,x_\infty} = 0$, following [58]. Note, this assumption neglects accumulation of bacteria at boundaries due to their persistent motion. However, since the accumulation only occurs within a thin region with thickness given by the persistence length v_0/ω, it is not relevant for the pulse propagation in the bulk, which we study here. To arrive at the conditions of equation (28), we consider the governing equations of the KS and PE model, separately. The second condition for c in equation (28) means that the chemical flux at the boundaries vanishes. For the KS model, the bacterial flux is $-D_{\text{eff}}\nabla\rho + \mathbf{v}_{\text{ch}}\rho$, which we identify from equations (18) and (20). The flux vanishes at the boundaries due to the first condition of equation (28) and since $\mathbf{v}_{\text{ch}} = 0$ for zero chemical gradient. For the PE model, equation (12) gives the bacterial flux $v_0\mathbf{P} - D\nabla\rho$, which also vanishes at the boundary due to the first condition of equation (28) and the vanishing polarization[5]. Finally, when integrating equation(16) the sink term can produce negative concentrations of the chemoattractant [75, 76]. To avoid this, we set the concentration c to zero whenever it would become negative. This allows the bacteria to fully degrade the chemoattractant without producing negative values for c.

When we solve our equations with real parameters, we rely on [36] and take the channel length $x_\infty = 10^5\,\mu$m and the initial decay length of the bacterial density as $x_0 = 50\ \mu$m. This ensures that at $t = 0$ 99% of the bacteria can be found within 200 μm at the channel end at $x_0 = 0$. To be concrete, we also assume a channel cross section $A = 500\ \mu\text{m} \times 100\ \mu\text{m}$ to calculate the initial number of bacteria $N_0 = \rho_0 x_0 A$, which we use as a parameter instead of ρ_0 in the following. We divide the channel length into 5×10^4 grid points so that the grid length is 2 μm and use the time step 0.01 s for integrating our equations in time. All the relevant parameters are given in table 1. Finally, we will also numerically solve the rescaled Keller–Segel equations (26) and (27) in order to explore the dependence on some of the relevant dimensionless parameters.

4. Traveling concentration pulses of bacteria

We first introduce the traveling bacterial pulse for a reference system using two values for the initial number of bacteria, then perform a systematic parameter study, and finally demonstrate a perfect match with the experimentally observed bacterial pulse reported in [36].

[5] Note, the correct treatment of the no-flux boundary condition in the PE model would take $\mathbf{n}\cdot\int\mathbf{J}_{\text{trans}}\mathbf{d}\mathbf{e} = 0$ and $\mathbf{n}\cdot\int\mathbf{J}_{\text{trans}}\mathbf{e}\mathbf{d}\mathbf{e} = 0$, where $\mathbf{n}$ is the unit vector normal to the bounding surface. In our geometry this implies $v_0P_x - D\partial\rho/\partial x = 0$ and $-v_0/d\ \rho + D\partial P_x/\partial x = 0$, where in the second condition we neglected the contribution from the quadrupole moment $\mathbf{Q}$.

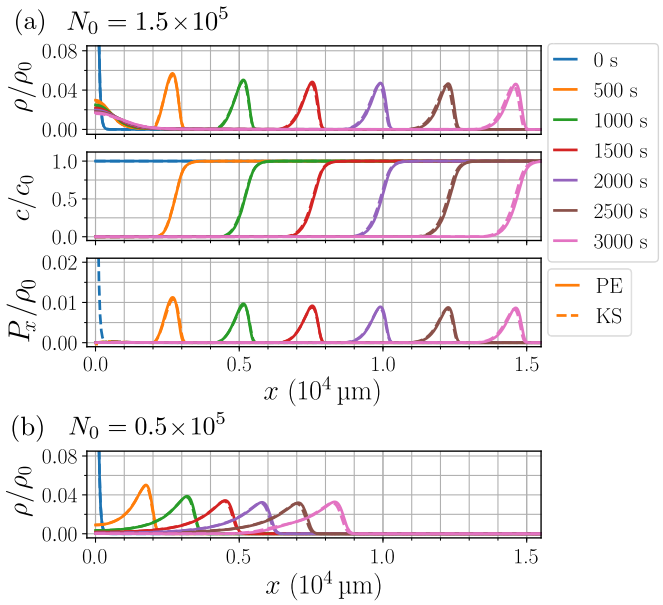

Figure 2. Bacterial pulse propagation: (a) snapshots of the bacterial density $\rho(x)$ (upper panel), the chemoattractant concentration field $c(x)$ (middle panel), and polarization $P_x(x)$ (bottom panel) at equally spaced times for the parameter set given in table 1. Solid lines represent the polarization extended model and dashed lines its adiabatic approximation, the generalized Keller–Segel model. (b) Bacterial density for a reduced number of bacteria $N_0 = 0.5 \times 10^5$ compared to the reference system.

Table 1. List of parameters used for the reference pulse in figure 2 and for the match to the experimental system shown in figure 6.

Parameter	Value figure 2	Value figure 6	References
D	0.2 μm^2 s^{-1}	Same	[35]
D_{rot}	0.06 s^{-1}	Same	[39]
α	0	1.67×10^{-4} s^{-1}	[36]
k	3.35×10^6 s^{-1}	Same	[64]
λ_{equ}	3 s^{-1}	Same	[36]
v_0	25 μm s^{-1}	Same	[36]
$\langle \cos\beta \rangle$	0.392	Same	[36]
D_c	8×10^2 μm^2 s^{-1}	Same	[36]
χ_0	0.64 $\lambda_{\mathrm{equ}} \delta v_0^{-1}$	Same	[36]
δ	600 μm	Same	[36]
c_0	1.26×10^6 μm^{-3}	2.61×10^6 μm^{-3}	—
c_t	$10^{-12}\, c_0$	$10^{-1}\, c_0$	—
A	5×10^4 μm^2	Same	[36]
x_0	50 μm	Same	[36]
N_0	1.5×10^5	1.5×10^5	[36]

4.1. Reference system

Figure 2(a) shows a series of snapshots of the bacterial density profile $\rho(x, t)$, the concentration field $c(x, t)$, and the polarization $P_x(x, t)$ at equally spaced times for realistic parameters of the *E.coli* bacterium listed in table 1. Solid lines represent numerical solutions of the polarization-extended model (PE) and dashed lines of the generalized Keller–Segel model (KS). Video S1 of the supplemental material is available online at stacks.iop.org/NJP/21/103001/mmedia. It shows an animation of the propagating profiles.

Clearly, while the bacteria consume the chemoattractant completely, a traveling pulse in the bacterial density forms that propagates with constant pulse speed $v_p = 4.68$ μm s^{-1}. It has a comparable width to the traveling step in the chemoattractant profile. In contrast to the bacterial solitons derived from the original KS model in [51], our bacterial pulse shows a small dispersion visible from the slight decrease of the pulse height. It is caused by bacteria that cannot follow the pulse at small chemoattractant concentrations since in our model the chemotactic drift velocity $\mathbf{v}_{\mathrm{ch}}$ of equation (20) has an upper bound. In contrast, in the original KS model $\mathbf{v}_{\mathrm{ch}}$ diverges at small chemoattractant concentrations [51], which allows all bacteria to stay in the traveling pulse. Thus, we demonstrate when one allows dispersion a singular chemotactic drift velocity is no longer necessary for

traveling pulses to occur. Note, already [66] used the KS model with a bounded chemotactic drift and observed traveling pulses which was ignored in more recent works [36, 54]. Instead, a second chemoattractant was proposed as explained in the introduction.

One realizes that the profiles generated from the KS and PE model are identical except in the beginning. We start with $P_x = 0$ in the PE model whereas in the KS model a non-zero polarization is calculated from equation (17). It is due to the initial gradient in the bacterial density. Thus, we conclude that the adiabatic limit $\frac{\partial P}{\partial t} \approx 0$ as a condition for deriving the generalized KS model is fulfilled. Indeed, the decorrelation or decay time $\omega^{-1} = 0.49$ s is much smaller than the characteristic time for the pulse propagation. For the latter, we approximately find 200 s for the pulse to travel its own width and the polarization always assumes its stationary value. Our finding also means that the kinetic models of [36, 41, 56], which work with the full one-particle distribution function $\psi(\mathbf{r}, \mathbf{e}, t)$, are not necessary to describe pulse propagation. They can be reduced to the Keller–Segel equations.

In figure 2(a) not all bacteria travel with the pulse but some remain at the initial location. This also occurs in the experiments of [6]. However, there the remaining bacteria perform chemotaxis in oxygen as a second chemoattractant and thereby initiate a secondary pulse. Since we do not incorporate another chemoattractant, the bacterial distribution at the initial location only broadens by diffusion. Finally, we mention previous numerical work on the KS model that also showed the bacteria left behind [66].

In their original work Keller and Segel derived an analytic expression for the speed of the bacterial soliton. It is a function of the number of bacteria in the soliton N_p, the consumption rate k, the cross section A, and the initial chemoattractant concentration c_0 [51]

$$v_p^{\mathrm{th}} = \frac{N_p k}{A c_0}. \tag{29}$$

In appendix C we demonstrate how this relation is derived. It is also valid in our case provided we can clearly identify an isolated pulse. Now, by integrating the bacterial density along the x direction at time $t = 2000$ s, we obtain $N_p = A \int \rho \mathrm{d}x = 0.88 \times 10^5$ bacteria in the pulse and for the number of bacteria left behind close to $x = 0$, $N_c = 0.57 \times 10^5$. Note, N_p and N_c do not add up to N_0 since there are also bacteria in the trail between the initial location and the pulse. Using N_p and the parameter values of the reference system from table 1 in equation (29), we obtain $v_p^{\mathrm{th}} = 4.69\ \mu\mathrm{m\ s}^{-1}$, which is in very good agreement with our numerical value of $v_p = 4.68\ \mu\mathrm{ms}^{-1}$.

In figure 2(b) we lower the number of bacteria N_0 by a factor of three. Now, all bacteria travel in the pulse and none are left behind. This suggests that the traveling pulse can only carry a certain number of bacteria and thus has a maximum carrying capacity. Indeed, in appendix C we show that the pulse speed v_p is bounded from above by the chemotactic drift speed of equation (20), which itself cannot grow to infinity since we bound the chemotactic response through the tumble rate. Thus, the number N_p of bacteria in the pulse, given in equation (29), cannot become arbitrarily large. We will investigate the maximum carrying capacity in more detail in the following parameter studies, where we use the two traveling pulses from figure 2 as a reference. For the traveling pulse in figure 2(b) we determine a smaller pulse speed of $v_p = 2.66\ \mu\mathrm{m\ s}^{-1}$. It matches very well with the theoretical prediction from equation (29) using $N_p = N_0 = 0.5 \times 10^5$. Video S2 of the supplemental material (available online at stacks.iop.org/NJP/21/103001/mmedia) shows an animation of the traveling profiles.

4.2. Parameter studies

4.2.1. Influence of bounded chemotactic drift

To keep the tumble rate positive, we introduced the chemotactic length δ in equation (4), which prevents the chemotactic drift velocity in equation (20) to become arbitrarily large. Furthermore, for the chemotactic response the lower chemical threshold c_t was introduced. In figure 3 we explore the influence of both parameters on the traveling bacterial pulse. The chemotactic length δ increases from left to right and the threshold concentration c_t from top to bottom. The reference system of figure 2(a) is in the center.

A smaller chemotactic length δ means that the bacterium can sense larger chemical gradients and that the drift velocity v_{ch} saturates at a larger value proportional to δ^{-1}. However, δ cannot be chosen arbitrarily small since then the tumble rate in equation (4) becomes negative. In this case our numerical solution scheme is unstable and the bacterial density becomes negative.

The length $\delta = 384\ \mu$m is close to the minimal value. In particular for small c_t nearly all bacteria travel in the pulse, none are left at the origin. As a result, the pulse travels the fastest. Increasing δ to 600 μm, it is clearly visible that some bacteria are left behind. Thus, the pulse contains less bacteria and, therefore, is slower. This is also in agreement with the smaller chemotactic drift velocity. Interestingly, for the smallest c_t we observe a second propagating pulse strongly decreasing in height. Finally, if we increase δ by a factor of 10–6000 μm, the majority of bacteria stay close to the initial location while only a smaller number of them travels in the pulse (note the 10 times smaller range of the vertical axis). Thus, the pulse speed is small and the pulse has not yet

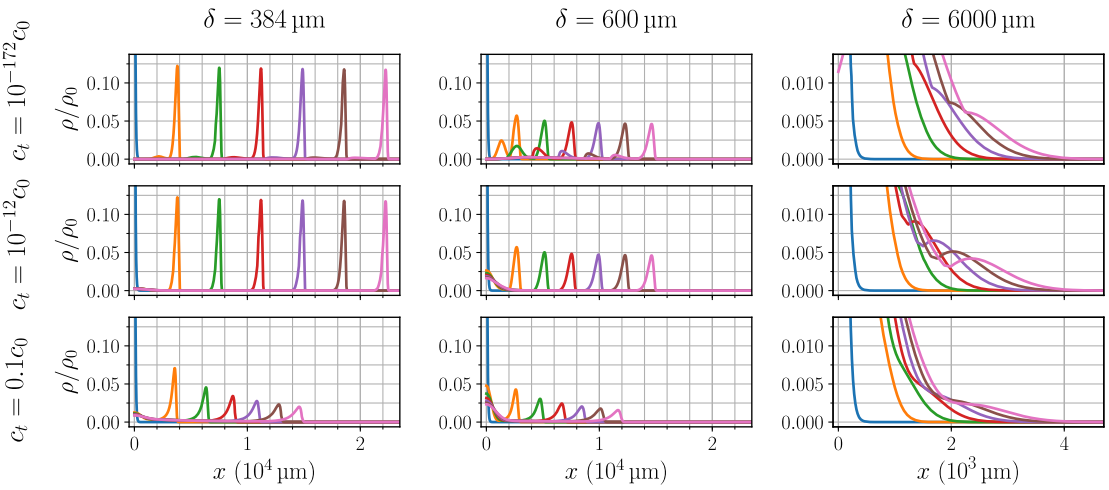

Figure 3. Rescaled bacterial density ρ/ρ_0 as a function of the chemotactic length δ and threshold concentration c_t. We increase δ from left to the right and c_t from top to bottom. The reference pulse from figure 2(a) is in the center. The color code for the different times is the same as in figure 2. Note the smaller ranges of the x and y axis in the last column.

separated from the non-propagating bacteria. In conclusion, increasing δ decreases the maximum carrying capacity significantly and makes the pulse slower.

Increasing the threshold concentration c_t from nearly zero to $c_t = 0.1c_0$ has three effects. First, the dispersion of the pulse increases which slows down the pulse. This is most notable when comparing the second to the third row. Second, the shape of the pulse becomes more asymmetric as bacteria at the rear flank cannot follow the pulse. Third, the number of bacteria left behind at the initial location increases slightly. In the upper middle plot we recognize that the threshold c_t is so low that the remaining bacteria can still travel by chemotaxis, although with a stronger dispersion as the first pulse. Finally, even for the vanishing threshold of the upper left plot a slight dispersion is visible. This again suggests that a true propagating soliton, for which the pulse shape does not vary in time, is not possible as long as the chemotactic drift velocity is bounded.

4.2.2. Quantitative study of the rescaled Keller–Segel equations

We now consider the rescaled Keller–Segel equations and study the propagating bacterial pulse in detail. Hence, we plot the rescaled pulse speed v_p, the pulse full width at half maximum Δx_h, and the pulse amplitude $\rho_{\max}/\rho_0$ as a function of the remaining parameters ρ_0/c_0, D_c/D_{eff} and $\chi_0(1 - \langle \cos\beta \rangle)$. Again, we neglect bacterial growth by setting $\tilde{\alpha} = 0$. Figure 4 shows all results and the relevant parameters are given in the figure caption.

In figure 4(a) we see that the pulse speed depends linearly on ρ_0/c_0 in agreement with the Keller–Segel prediction of equation (29) but then saturates at a constant value. The reference pulse from figure 2(b) (purple disc), where all bacteria travel with the pulse, is located in the linear regime, while the reference pulse from figure 2(a) (orange star), where some bacteria remain close to the origin, propagates in the saturated regime. Thus, in the first case adding more bacteria to the system increases the number of bacteria in the traveling pulse and speeds it up. In contrast, in the second case additional bacteria remain close to the initial location. Thus, the traveling concentration pulse has a maximum carrying capacity N^* with respect to the amount of bacteria it can carry while further bacteria exceeding the carrying capacity are left behind. This is in agreement with appendix C, where we derive an upper bound for N^*. The transition between both regimes occurs at the critical ratio $(\rho_0/c_0)^*$. To illustrate the transition, we discuss the following scenario. Lowering c_0 at constant ρ_0 speeds up the pulse in the linear regime since bacteria degrade the chemoattractant faster and in agreement with equation (29). However, once $(\rho_0/c_0)^*$ is reached, the pulse looses bacteria to keep the pulse velocity constant, again according to equation (29). Thus the carrying capacity of the pulse decreases when c_0 decreases below a treshold.

The ratio ρ_0/c_0 also influences the pulse shape. In the linear regime of increasing ρ_0/c_0 the pulse becomes narrower while its absolute height $\rho_{\max}$ roughly increases with ρ_0^2. When reaching the saturation regime, the pulse width stays constant as should $\rho_{\max}$. Thus for the relative height we find $\rho_{\max}/\rho_0 \propto (\rho_0/c_0)^{-1}$.

In figure 4(b) we show the pulse speed does not significantly depend on the ratio of diffusion constants, D_c/D_{eff}, for both study cases I (blue stars) and II (green circles). This is in contrast to [77] where the authors proposed a correction term to equation (29), which predicts a decrease of the pulse speed with increasing D_c. However, when examining the bacterial pulse profile, we observe that for larger D_c/D_{eff} the pulse needs more time to form. It needs more time to consume all the chemoattractant at the origin due to the larger diffusive flux

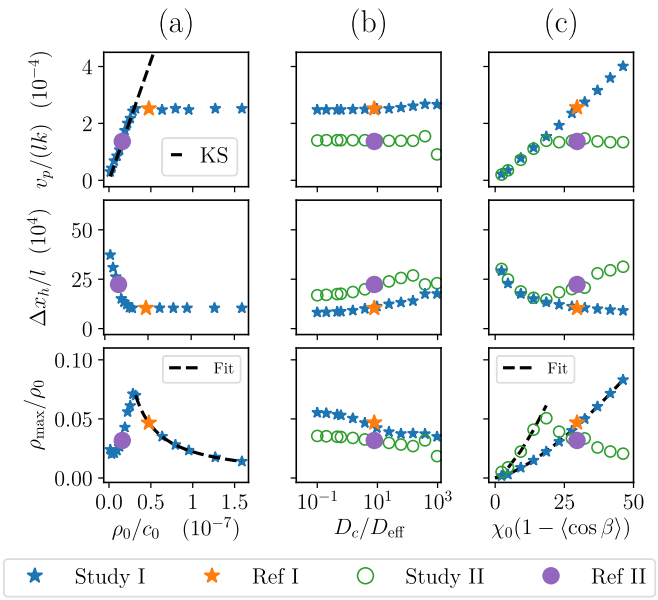

Figure 4. Parameter study for the traveling bacterial concentration pulse. The rescaled pulse speed v_p (first line), full width at half maximum of the pulse Δx_h (second line), and pulse amplitude $\rho_{\max}/\rho_0$ (third line) are plotted as a function of the rescaled parameters ρ_0/c_0 (a), D_c/D_{eff} (b), and $\chi_0(1-\langle\cos\beta\rangle)$ (c). The values are determined at rescaled time $\tilde{t}=10^{10}$, where pulse propagation is well established. When not varied, the following rescaled parameters are used: $\rho_0/c_0=4.76\times10^{-8}$ (blue stars, study I) and $\rho_0/c_0=1.59\times10^{-8}$ (green circles, study II), $D_c/D_{\text{eff}}=7.84$, $\chi_0(1-\langle\cos\beta\rangle)=29.6$, $\tilde{\delta}=1.09\times10^5$, $\tilde{c}_t=10^{-12}$, and $\tilde{\alpha}=0$. The reference pulses from figures 2(a) and (b) are marked with orange stars (Ref I) and purple discs (Ref II), respectively. The dashed line in the curve $\rho_{\max}$ versus ρ_0/c_0 is a fit to $y(x)=C/x$ with $C=2.22\times10^{-9}$ while the dashed lines in the curves $\rho_{\max}$ versus $\chi_0(1-\langle\cos\beta\rangle)$ are fits to $y(x)=Ax^B$ with $A=3.53\times10^{-4}$, $B=1.42$ (blue stars) and $A=10.4\times10^{-4}$, $B=1.43$ (green circles).

of chemoattractant into the depleted areas. But once the bacteria have fully degraded the chemoattractant, the pulse propagates with the same speed v_p independent of D_c. For increasing D_c/D_{eff} the width of the pulse also increases while the amplitude decreases. However, both trends are not very significant since pulse width and amplitude do not even change by a factor of two while D_c/D_{eff} is varied over four orders of magnitude. Finally, we note the relevant length scale $l=\sqrt{D_{\text{eff}}/k}$ to depend on the effective bacterial diffusion constant D_{eff} and thus find $v_p\propto\sqrt{D_{\text{eff}}}$. Moreover, the pulse width increases significantly with D_{eff} while the absolute height increases only slightly.

Figure 4(c) shows the results when the chemotactic parameter $\chi_0(1-\langle\cos\beta\rangle)$ is varied. For values larger than 50 the numerical scheme becomes unstable similar to the instability in the chemotactic length δ already discussed in section 4.2.1. The pulse speed increases linearly in the chemotactic parameter for the study case I (blue stars) and also for the study case II (green circles) in the range $\chi_0(1-\langle\cos\beta\rangle)<20$. To understand this finding, we looked in detail at the bacterial profiles. In study case II we find that with increasing $\chi_0(1-\langle\cos\beta\rangle)$ more and more bacteria from the vicinity of the initial location enter the pulse, which according to equation (29) then speeds up. Thus we conclude for the maximum carrying capacity of the pulse, $N^*\propto\chi_0(1-\langle\cos\beta\rangle$. A similar observation in connection with the scenario of figure 4(b) gives $N^*\propto\sqrt{D_{\text{eff}}}$. Note that our results are in contrast to [78] which found $v_p\propto\sqrt{\chi_0}$. In study case II (green circles) we start with a smaller number of bacteria. Thus, at $\chi_0(1-\langle\cos\beta\rangle)\approx20$ all bacteria have entered the pulse, which then travels with constant speed when $\chi_0(1-\langle\cos\beta\rangle)$ is further increased. Finally, with growing chemotactic parameter the width of the traveling pulse decreases in the study case I (blue stars). The curve of study case II (green circles) follows this trend until the pulse speed becomes constant and then steadily increases.

For the pulse amplitude of the two study cases the behavior of the curves are inverted compared to the pulse width. The curves are well fitted by $y(x)=Ax^B$, where the constants A differ approximately by a factor of three. This is the factor by which the density ratios ρ_0/c_0 of study cases I and II differ. The factor of three appears since we plot the reduced amplitude $\rho_{\max}/\rho_0$. The exponents are nearly the same. The amplitude of the study case II (green circles) decreases for $\chi_0(1-\langle\cos\beta\rangle>20$ and thereby compensates the increasing pulse width as the number of bacteria in the pulse is constant.

4.2.3. Influence of growth rate α

Finally, we investigate the influence of the growth term in the Keller–Segel equation (18). Figure 5 shows propagating pulses for three different growth rates α, while the other parameters are chosen as in the reference

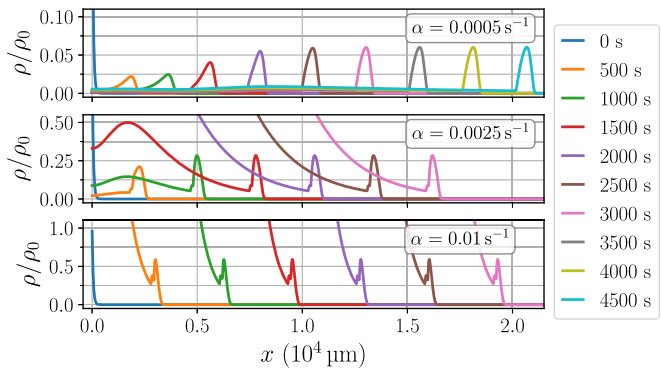

Figure 5. Propagating bacterial pulses for three different growth rates α. Other parameters are the same as the reference pulse of figure 2(b) with an initial population of $N_0 = 0.5 \times 10^5$.

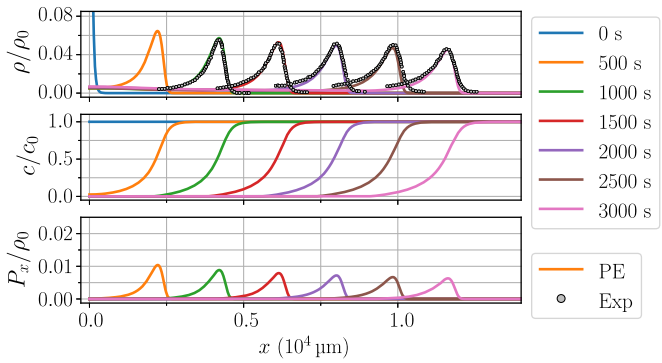

Figure 6. Comparison of the experimental traveling pulse (gray circles) from figure 1(b) in [36] and the simulated pulse using our model (colored lines) with parameters given in table 1. Both bacterial density profiles are indicated in the upper panel at different times, the chemical field c is shown in the middle panel, and the polarization P_x in the lower panel. The pulse speeds in both cases are identical: $v_p = 3.8\ \mu\mathrm{m\ s}^{-1}$.

system but with the reduced initial number of bacteria $N_0 = 0.5 \times 10^5$. It is below the maximum carrying capacity of the pulse and was used in figure 2(b).

Consequently, in the upper panel the pulse grows due to the non-zero growth rate and speeds up in time until the maximum carrying capacity is reached at around 2600 s. Then, the pulse propagates with constant shape like a perfect soliton. However, in our case the pulse leaves a trail of bacteria behind, which originates from the continuous bacterial growth.

In the middle and lower panel, the maximum carrying capacity is reached after 1000 s and 50 s, respectively. Interestingly, the pulse does no longer separate from the broad distribution of bacteria, which spreads from the initial location, but rather sits on top of the distribution's right flank. In the lower panel the pulse is fastest and its amplitude is highest. This comes from the fact that the broad distribution around the origin contains much more bacteria compared to the middle panel and, thus, more bacteria actively take part in the degradation of the chemoattractant. As a consequence, the pulse propagates faster.

Last, we observe that with increasing growth rate the pulse becomes more peaked. This is reminiscent to figures 4(a) and (c), where a faster pulse has a smaller pulse width.

4.3. Matching the experimental pulse

Figure 6 (upper panel) shows the traveling bacterial concentration pulse recorded in the experiments of [36] and compares it to the numerical solution of our polarization extended model. Both propagating pulses agree very well in shape and in speed $v_p = 3.8\ \mu\mathrm{m\ s}^{-1}$. We extracted the experimental data from figure 1(b) in [36] and in our model mainly used parameters from the same publication including a non-zero growth rate but also added missing values from [39, 64]. Moreover, a realistic value for the sensing threshold $c_t = 2.61 \times 10^5\ \mu\mathrm{m}^{-3} = 0.1 c_0$ was chosen [64]. This was necessary to match the asymmetry and dispersion of the pulse. The full parameter set is given in table 1.

5. Discussion and conclusions

In the first part of this article we demonstrated how to derive the celebrated Keller–Segel equation using a generalized Smoluchowski equation for the full distribution function in position and orientation and a multipole expansion. An important ingredient is the bacterial tumble rate in a chemical field. We derived the known Markovian response theory for the mean tumble rate starting from the classical chemotaxis strategy based on temporal sensing in order to explain experimental results from [39]. Our expression for the tumble rate includes logarithmic sensing and we added a lower chemical threshold and an upper bound for the chemotactic response to keep the tumble rate positive. The multipole expansion provides a polarization extended model (PE) from which we derived the Keller–Segel equation in the adiabatic limit, where the bacterial polarization instantly follows variations in the density. We thereby obtain microscopic expressions for the diffusion coefficient and the chemotactic drift velocity. Due to the bounded chemotactic response the inherent and unrealistic singularity in the drift velocity is removed.

Our detailed study of the traveling bacterial pulse shows that its characteristic time is much larger than the relaxation time of the bacterial polarization. Thus, PE and KS model provide identical results except for the initial fields and we conclude that the full Smoluchowski equation as used for example in [36, 56] is not necessary. This drastically reduces the computational effort and allowed us to perform extensive numerical studies of the bacterial pulse propagation.

We find that due to the upper bound of the chemotactic velocity the traveling pulse can only carry a limited number of bacteria. To the best of our knowledge such a *maximum carrying capacity* has not yet been reported in the context of traveling bacterial pulses. In particular, it is not predicted by the analytic soliton solution of the original Keller–Segel model [51]. Another consequence of the upper bound of the chemotactic velocity is an effective dispersion of the pulse. While propagating, the pulse leaves a trail of bacteria behind and hence the pulse height decreases and the width expands. This is consistent with results from [66]. The loss of bacteria can be compensated by a non-zero growth rate and we have seen that soliton-like pulses, which propagate with constant shape, are possible.

Exploiting a rescaled version of our KS model, we quantify how pulse speed, pulse width, and pulse amplitude depend on the different unitless parameters. We mention some key results. First, throughout our parameter study we find that the analytic soliton solution of the original KS model still provides a correct estimate for the pulse speed as a function of the number of bacteria in the pulse. Second, we find the maximum carrying capacity to be proportional to the chemotactic strength $\chi_0(1 - \langle \cos\beta \rangle)/\tilde{\delta}$ and $\sqrt{D_{\mathrm{eff}}}$. As a consequence these parameters affect the pulse speed as long as there are sufficient bacteria in the system so that the maximum carrying capacity is reached. Third, the diffusion coefficient of the chemoattractant does not influence the pulse speed as predicted in a theoretic model in [77]. The pulse only takes longer to eat up all the chemoattractant at the origin due to the larger diffusive flux of chemoattractant into depleted areas.

Finally, we show that our simulated pulse propagation is able to match quantitatively the traveling bacterial pulse in the exeriments of [36] in speed and shape. In contrast to the models used in [54] and [36], we do not need a second chemoattractant to generate a traveling concentration pulse as a solution of our generalized KS model.

We mention four directions into which our approach can be extended. First, so far we did not explore the full PE model, which will be relevant for dynamic processes with typical time scales of the order of $1/\omega$. In future works it would be interesting to explore the possibility of having the bacterial polarization as an independent field and its potential to induce complex dynamics. For example, the alignment or polarization of magnetotatic bacteria can be controlled by an external magnetic field [79, 80], which offers the possibility to address polarization as an independent field variable, e.g. by a time-varying external stimulus. The dependence of cell characteristics on polarization could also evoke a feedback loop in highly nonlinear equations. For example, it was shown that the nutrient uptake of bacteria depends on cell shape [81], meaning that the consumption rate may depend on the polarization, which then influences chemotaxis [82]. For Janus colloids with effective phoretic repulsion this can generate interesting collective dynamics on times much smaller than the characteristic time scale of the bacterial pulse [29]. Finally, in complex geometries with characteristic lengths similar to the persistence length of the bacterium, we expect the polarization equation also to become important.

Second, to describe the multiple pulses that have been observed in experiments with several nutrients [6, 83], one can extend our model by coupling the bacterial density to several nutrient fields. Bacteria that are left behind by the first pulse can then perform chemotaxis in a second nutrient field and thereby create a second pulse.

Third, in our generalized Smoluchowski equation the swimming speed is a constant as it is commonly done for the *E.coli* bacterium also during chemotaxis [33, 35, 40]. However, some bacteria are known to couple their swimming speed to the concentration of a chemical field [84–86], a strategy which is called chemokinesis. Reference [58] derived coupled equations for bacterial polarization and density from a Smoluchowski equation where the swimming velocity depends on the chemical concentration. It is certainly interesting to extend our

theory in order to investigate the combined effect of chemokinesis and chemotaxis. A cell that performs both strategies is the sperm cell [44].

Finally, it would be interesting to extend our approach to chemoattractants to which *E.coli* is not perfectly adapted such as serine [33, 40, 87]. For this chemoattractant the mean tumble rate drops as the concentration of serine increases. Thus, when swimming up a chemical gradient, the chemotactic velocity increases [87]. In our generalized KS model, the effective diffusion coefficient of bacteria D_{eff}, which directly depends on the tumble rate λ_{equ}, now is enhanced in front of the pulse as runs are longer, while it is smaller in the back of the pulse where runs are shorter. This should affect the pulse propagation and indeed, experiments with serine showed that below a certain strength of the chemical gradient traveling pulses do not form [88].

Acknowledgments

Fruitful discussions with J-T Kuhr are acknowledged. This work was supported by the German Research Foundation (DFG) within the research training group GRK1558, the RISE Germany Program of DAAD, and the Open Access Publication Fund of TU Berlin.

Appendix A. Markovian response theory for tumble rate

Equation (1) describes the non-Markovian linear response of the tumble rate on the concentration history of the bacterial trajectory $c(\mathbf{r}(t'))$. Now, by averaging over all possible trajectories that arrive at location $\mathbf{r}$ with orientation $\mathbf{e}$, we are able to derive a Markovian response theory for the mean tumble rate. We make use of the fact that rightward and leftward tumbling is equally probable, thus the tumble angle distribution is an even function, $P(\mathbf{e} - \mathbf{e}') = P(\mathbf{e}' - \mathbf{e})$. This has indeed been measured for *E.coli* in experiments [33, 39, 40]. In the following, we derive equation (2) from the main text.

We start with repeating the expression for the tumble rate from the linear response theory:

$$\lambda(t) = \lambda_{\mathrm{equ}} - \int_{-\infty}^{t} R(t - t')\, c(\mathbf{r}(t'))\mathrm{d}t'. \tag{A1}$$

In the following, we will use three key properties of the response function $R(\tau)$ that were measured in experiments [34, 38, 62]. First, starting from $\tau = 0$ it is non-zero over a time interval $\tau_m \lessapprox 15$ s, which we call the memory time. Second, it fulfills $\int_{-\infty}^{0} R(\tau)\mathrm{d}\tau = 0$, which means the tumble rate does not depend on the absolute chemical concentration (perfect adaptation). Third, it is inversely proportional to the adaptation concentration, $R(t - t') = \tilde{R}(t - t')/c_a$. Adaption occurs during the memory time, thus we can set $c_a = c(\mathbf{r}(t))$. Taking these properties into account, we will use the approximation $\int_{-\infty}^{0} R(\tau)f(\tau)\mathrm{d}t \approx 1/c_a \int_{-\tau_m}^{0} \tilde{R}(\tau)f(\tau)\mathrm{d}\tau$. In particular, due to perfect adaption any additive constant in $f(\tau)$ will not contribute to the integral.

To evaluate equation (A1), we need an expression for $c(\mathbf{r}(t'))$. Therefore, we perform a Taylor expansion around the current position $\mathbf{r}(t) = \mathbf{r}_t$ and locally approximate the chemical field by

$$c(\mathbf{r}') = c(\mathbf{r}_t) + \boldsymbol{\nabla} c \cdot (\mathbf{r}' - \mathbf{r}_t), \tag{A2}$$

where we used $\mathbf{r}' = \mathbf{r}(t')$. In the following derivation, all locations $\mathbf{r}'$ that contribute to the integral in equation (A1) should be close to the current location $\mathbf{r}_t$ so that the linear approximation is valid. Moreover, we assume that temporal variations of the chemical field are negligible within the memory time τ_m so that $\boldsymbol{\nabla} c$ is constant. Both requirements are justified for the bacterial pulse. On the one hand, the mean run length of bacteria is much smaller than the width of the step in the chemoattractant concentration, and on the other hand on times comparable to τ_m the step hardly moves.

Using equation (A2) in (A1), we obtain

$$\lambda(t) = \lambda_{\mathrm{equ}} - \boldsymbol{\nabla} c/c_a \cdot \int_{t-\tau_m}^{t} \tilde{R}(t - t')\, \mathbf{r}(t')\mathrm{d}t', \tag{A3}$$

where we applied the property of perfect adaption to set $\int_{-\tau_m}^{t} R(t - t')[c(\mathbf{r}_t) - \boldsymbol{\nabla} c(t) \cdot \mathbf{r}_t]\mathrm{d}t' = 0$ and that $\boldsymbol{\nabla} c$ is constant within the memory time τ_m.

To proceed, we write the trajectory of a bacterium that swims with constant velocity v_0 along the direction given by unit vector $\mathbf{e}(t)$ as $\mathbf{r}(t) = \mathbf{r}(t') + v_0 \int_{t'}^{t} \mathbf{e}(t'')\mathrm{d}t''$, where the bacterium has been at location $\mathbf{r}(t')$ before reaching $\mathbf{r}(t)$, thus $t' \leqslant t$. In the following, we use it in the form

$$\mathbf{r}(t') = \mathbf{r}(t) + v_0 \int_t^{t'} \mathbf{e}(t'')\mathrm{d}t''. \tag{A4}$$

Changes in the swimming direction due to rotational diffusion are much smaller than due to tumbling. Consequently, the trajectory of the bacterium becomes a sequence of straight runs and instantaneous tumble events. Denoting tumble events by index i, the tumble time t_i, and $\mathbf{e}_i$ the direction prior to tumble event i, we can write the orientation vector in equation (A4) at any time $t'' < t$ with the help of a telescope sum:

$$\mathbf{e}(t'') = \mathbf{e}(t) + \sum_{i=1}^{n}(\mathbf{e}_i - \mathbf{e}_{i-1}) = \sum_{i=0}^{n}(\mathbf{e}_i - \mathbf{e}_{i-1}). \tag{A5}$$

Here we set $\mathbf{e}_0 = \mathbf{e}(t)$ for the current direction after the last tumble event $i = 1$ and $\mathbf{e}_{-1} = \mathbf{0}$ is used. The number of tumble events in the time interval $t - t''$ is n and we number the tumble events backwards in time.

Now, we determine the mean tumble rate $\langle\lambda(t)\rangle$ by averaging the right-hand side of equation (A3) over an ensemble of bacterial trajectories $\mathbf{r}(t')$ that all reach the position $\mathbf{r}(t)$ with swimming direction $\mathbf{e}(t)$. For this, we first have to evaluate $\langle\mathbf{e}(t'')\rangle$ in equation (A4) by averaging over n independent tumble events and considering that n is a random variable. It is determined by the probability distribution $P(n, t - t'')$ of having n tumble events in the time interval $t - t''$. We can thus write

$$\langle\mathbf{e}(t'')\rangle = \sum_{n=0}^{\infty} P(n, t - t'')\sum_{i=0}^{n}\langle\mathbf{e}_i - \mathbf{e}_{i-1}\rangle. \tag{A6}$$

Note, for a constant tumble rate $P(n, t - t'')$ becomes a Poisson distribution. To calculate the mean tumble direction $\langle\mathbf{e}_i - \mathbf{e}_{i-1}\rangle$ we use the probability distribution $P(\mathbf{e}_{i-1} - \mathbf{e}_i)$ from the main text and calculate the first moment as in equation (11) but now with respect to the incoming direction $\mathbf{e}_i$ of the tumble event. This gives $\langle\mathbf{e}_i\rangle = \int \mathbf{e}_i P(\mathbf{e}_{i-1} - \mathbf{e}_i)\mathrm{d}\mathbf{e}_i = \langle\cos\beta\rangle\mathbf{e}_{i-1}$, where the tumble angle is determined by $\cos\beta = \mathbf{e}_{i-1}\cdot\mathbf{e}_i$ and we used that $P(\mathbf{e}_{i-1} - \mathbf{e}_i)$ is an even function meaning that left- and rightward tumbles are equally probable. Repeating the formula for $\langle\mathbf{e}_i\rangle$ for the whole sequence of tumble events, we finally have $\langle\mathbf{e}_i\rangle = \langle\cos\beta\rangle^i\mathbf{e}(t)$ and the telescope sum in equation (A6) becomes

$$\begin{aligned}\sum_{i=0}^{n}\langle\mathbf{e}_i - \mathbf{e}_{i-1}\rangle &= \sum_{i=0}^{n}\langle\mathbf{e}_i\rangle - \langle\mathbf{e}_{i-1}\rangle = \mathbf{e}(t) - \mathbf{0} + \sum_{i=1}^{n}\langle\cos\beta\rangle^i\mathbf{e}(t) - \langle\cos\beta\rangle^{i-1}\mathbf{e}(t)\\ &= \langle\cos\beta\rangle^n\mathbf{e}(t).\end{aligned} \tag{A7}$$

Combining the last two equations yields

$$\langle\mathbf{e}(t'')\rangle = \sum_{n=0}^{\infty} P(n, t - t'')\langle\cos\beta\rangle^n\mathbf{e}(t), \tag{A8}$$

where the only remaining orientation vector is the current one, $\mathbf{e}(t)$. In general, the probability distribution $P(n, t - t'')$ is a complex quantity as it depends on the tumble rates at previous times. Only for weak chemotaxis we can approximate the tumble rate by the constant value λ_{equ} and P becomes the Poisson distribution

$$P(n, t - t'') = \frac{[\lambda_{\mathrm{equ}}(t - t'')]^n}{n!}\mathrm{e}^{-\lambda_{\mathrm{equ}}(t-t'')}. \tag{A9}$$

The weak-chemotaxis approximation was used, e.g. by Locsei in [63]. However, knowing the exact form of $P(n, t - t'')$ is not relevant for our further argumentation.

Now, with equations (A8) and (A4) we can formulate the average location

$$\langle\mathbf{r}(t')\rangle = \mathbf{r}(t) + v_0\int_t^{t'}\sum_{n=0}^{\infty} P(n, t - t'')\langle\cos\beta\rangle^n\mathrm{d}t''\ \mathbf{e}(t). \tag{A10}$$

Using it in the tumble rate (A3), we finally obtain

$$\langle\lambda\rangle = \lambda_{\mathrm{equ}} - \chi_0 v_0\mathbf{e}(t)\cdot\frac{\boldsymbol{\nabla}c}{c_a} \tag{A11}$$

with

$$\chi_0 = \int_{t-\tau_m}^{t}\int_t^{t'}\sum_{n=0}^{\infty} P(n, t - t'')\langle\cos\beta\rangle^n\mathrm{d}t''\tilde{R}(t - t')\mathrm{d}t'. \tag{A12}$$

Setting $c_a = c(\mathbf{r})$ we then recover equation (2) from the main text. It is clear that χ_0 is a complicated quantity, which depends on the history of all trajectories, we average over. In the article we take a more pragmatic approach. We take χ_0 as a constant and concentrate on how the tumble rate depends on $\mathbf{e}(t)\cdot\boldsymbol{\nabla}c/|\boldsymbol{\nabla}c| = -\cos\theta$. This dependence was measured in experiments as we show in the plot of figure 1, right reproduced from [39].

Locsei in [63] calculated the chemotactic drift speed v_{ch} in the weak-chemotaxis approximation using an explicit form for the reponse function. We can reproduce his formula for v_{ch}, which demonstrates that our

approach agrees with his work. For weak chemotaxis equation (A9) is valid. Following [89] we can also include rotational diffusion and obtain for the mean orientation

$$\langle \mathbf{e}(t'')\rangle = \mathrm{e}^{-\lambda_{\mathrm{equ}}(1-\langle\cos\beta\rangle)(d-1)D_{\mathrm{rot}}(t-t'')}\mathbf{e}(t), \tag{A13}$$

which replaces equation (A8). Note that in the exponent we recover the relaxation rate $\omega = \lambda_{\mathrm{equ}}(1 - \langle\cos\beta\rangle) + (d-1)D_{\mathrm{rot}}$ from equation (14) in the main text. We will further use it. Now the exponential function of the last equation becomes the integrand in equation (A12). Integrating over t'', we arrive at

$$\chi_0 = \int_{t-\tau_m}^{t} \frac{\mathrm{e}^{-\omega(t-t')}}{\omega}\tilde{R}(t-t')\mathrm{d}t'. \tag{A14}$$

The parameter χ_0 appears in equation (20) for the chemotactic drift speed $v_{\mathrm{ch}} = |\mathbf{v}_{\mathrm{ch}}|$, which we reproduce here without the threshold and saturation terms:

$$v_{\mathrm{ch}} = \frac{v_0^2(1-\langle\cos\beta\rangle)}{\omega d}\chi_0\frac{|\nabla c|}{c}. \tag{A15}$$

We choose the same parametrization for the response function as [63]

$$\tilde{R}(t) = \frac{2\zeta\lambda_{\mathrm{equ}}^3}{3}\mathrm{e}^{-\lambda_{\mathrm{equ}}t}\left[1 - \frac{\lambda_{\mathrm{equ}}t}{2} - \left(\frac{\lambda_{\mathrm{equ}}t}{2}\right)^2\right], \tag{A16}$$

where ζ quantifies the strength of the response function. Calculating χ_0 from equation (A14) we finally arrive at

$$v_{\mathrm{ch}} = \frac{\zeta v_0^2\lambda_{\mathrm{equ}}^3(1-\langle\cos\beta\rangle)(2\omega+3\lambda_{\mathrm{equ}})}{9\omega[\omega+\lambda_{\mathrm{equ}}]^3}\frac{|\nabla c|}{c}, \tag{A17}$$

were we used the dimension $d = 3$. This expression agrees with equation (57) in [63] up to the factor $1/c$, which resulted from setting $R = \tilde{R}/c$ in the beginning and which [63] did not introduce.

Appendix B. Parameter dependence of the tumble rate

We restate the relation for the tumble rate

$$\lambda(\mathbf{r}, \mathbf{e}) = \lambda_{\mathrm{equ}} - \chi_0\frac{v_0}{\delta}\tanh\left(\frac{c}{c_t}\right)\tanh\left(\delta\frac{|\nabla c|}{c}\right)\mathbf{e}\cdot\hat{\mathbf{s}}, \tag{B1}$$

where we use the normalized gradient direction $\hat{\mathbf{s}} = \frac{\nabla c}{|\nabla c|}$. We also introduce the orientation angle θ between $\mathbf{e}$ and the negative chemical gradient

$$\cos\theta = -\mathbf{e}\cdot\hat{\mathbf{s}}. \tag{B2}$$

To illustrate the effect of the additional parameters δ and c_t associated with the hyperbolic tangent function, we plot the tumble rate as a function of the chemical concentration c in figure C1 varying different parameters. Already in figure C1(a), where we vary c_t, we recognize the main features by identifying three regions. For concentrations well below the sensing threshold, $c \ll c_t$, the tumble rate approaches its equilibrium value. This

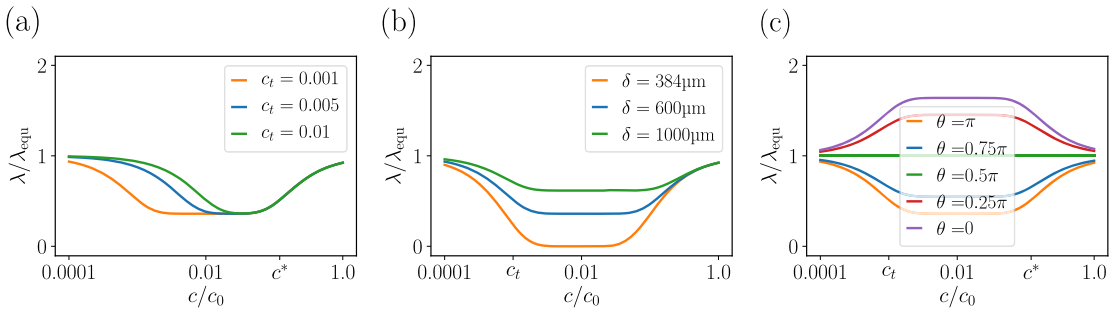

Figure C1. Semi-logarithmic plot of the normalized tumble rate $\lambda/\lambda_{\mathrm{equ}}$ as a function of the chemical concentration c for different c_t (a), δ (b), and θ (c). We always choose $|\nabla c| = 2\times10^{-4}\ \mu\mathrm{m}^{-1}c_0$, close to the maximum slope of the chemical step in figure 2(a). If not stated otherwise, we also keep the values of the other parameters constant: $\frac{\chi_0 v_0}{\lambda_{\mathrm{equ}}} = 384.0\ \mu$m, $c_t = 10^{-3}\ c_0$, $\delta = 600\ \mu$m, and $\theta = \pi$. The saturation of the chemotactic response occurs below $c^* = |\nabla c|\delta$ and c_t is the chemotactic sensing threshold.

also ensures a smooth transition to the case where no chemoattractant is present, $\lambda(c=0)=\lambda_{\mathrm{equ}}$. For increasing concentrations but smaller than $c^*=\delta\nabla c$, the chemotactic response saturates to a constant value below λ_{equ}. Note that the tumble rate cannot become negative as long as the parameters satisfy

$$\frac{\chi_0 v_0}{\delta\lambda_{\mathrm{equ}}}<1. \tag{B3}$$

This relation must be also fulfilled when the bacterial swimming speed varies. Finally, increasing c further beyond c^*, we recover the $1/c$ dependence from the original Keller–Segel model.

In figure C1(b) we vary the chemotactic length δ, which has two effects. First, the concentration $c^*=\delta\nabla c$, where the transition to the conventional $1/c$ dependence occurs, increases with δ. Note that $\delta=600\ \mu$m used for the pulse propagation in figure 2(a) guarantees that we are in the conventional $1/c$ regime. Second, the maximum tumble-rate variation $\chi_0 v_0/\delta$ scales with δ^{-1}, which is clearly visible in figure C1(b). In fact, at $\delta=384\ \mu$m the tumble rate becomes zero. Finally, in figure C1(c) we illustrate that the maximum tumble-rate variation behaves like $\cos\theta\ \chi_0 v_0/\delta$.

Appendix C. Upper bound for the maximum carrying capacity

From the Keller–Segel equations (18) and (19) in 1D we derive the equations to describe a bacterial pulse. Since it should propagate with constant shape, one writes the bacterial and chemical densities as functions of the pulse variable $\xi=x-v_p t$ and obtains [51]

$$-v_p\frac{\partial\rho}{\partial\xi}=D_{\mathrm{eff}}\frac{\partial^2\rho}{\partial\xi^2}-\frac{\partial}{\partial\xi}v_{\mathrm{ch}}\rho, \tag{C1}$$

$$-v_p\frac{\partial c}{\partial\xi}=D_c\frac{\partial^2 c}{\partial\xi^2}-k\rho. \tag{C2}$$

The boundary conditions at $\xi\to\pm\infty$ are $\rho=0$, $\frac{\partial\rho}{\partial\xi}=0$, $c=c_0/0$, and $\frac{\partial c}{\partial\xi}=0$. Following the approach of [51], we integrate the second equation from $-\infty$ to ∞ and obtain the Keller–Segel relation for the pulse speed v_p:

$$v_p=\frac{kN_p}{Ac_0}, \tag{C3}$$

where N_p/A is the number of bacteria in the pulse per unit area.

Now, we can derive another relation for the pulse speed by integrating equation (C1) from ξ to ∞

$$v_p=v_{\mathrm{ch}}(\xi)-D_{\mathrm{eff}}\frac{\partial\rho}{\partial_\xi}/\rho. \tag{C4}$$

This equation has to be fulfilled for all ξ, in particular, also in the rear of the pulse. Here $\frac{\partial\rho}{\partial\xi}$ is positive and so is the second term on the rhs of the last equation. Therefore, the pulse speed always has to be smaller than the chemoctactic drift speed, which itself has a maximum value $v_{\mathrm{ch,max}}$. Thus we obtain an upper bound for the pulse speed

$$v_p<v_{\mathrm{ch,max}}. \tag{C5}$$

Inserting v_p from equation (C3), we finally obtain an upper bound for the maximum carrying capacity

$$N^*<\frac{Ac_0}{k}v_{\mathrm{ch,max}}. \tag{C6}$$

Appendix D. Multipole expansion with bias in the tumble angle

Following the same steps as in the multipole expansion without angle bias, we average equation (8) over all orientations $\mathbf{e}$ using equation (22) and obtain

$$\frac{\partial\rho}{\partial t}=-\nabla\cdot(v_0\mathbf{P})\ +D\nabla^2\rho+\alpha\rho. \tag{D1}$$

Similarly, we compute the polarization $\int\mathbf{e}$ equation (8) $\mathrm{d}\mathbf{e}$ using equations (23) and (24) and with $\hat{\mathbf{s}}=\frac{\nabla c}{|\nabla c|}$ we obtain

$$\frac{\partial \mathbf{P}}{\partial t} = -v_0 \nabla \cdot \mathbf{Q} - \frac{v_0}{d}\nabla\rho + D\nabla^2\mathbf{P} - [D_{\mathrm{rot}}(d-1) + (1-\overline{\Theta})\lambda_{\mathrm{equ}}]\mathbf{P} + (1-\overline{\Theta}_0)\chi\left(\frac{|\nabla c|}{c}\right)\mathbf{Q}\cdot\hat{\mathbf{s}} + \frac{1-\overline{\Theta}_0}{d}\chi\left(\frac{|\nabla c|}{c}\right)\rho\,\hat{\mathbf{s}} + \lambda_{\mathrm{equ}}\sigma\left(\frac{|\nabla c|}{c}\right)\mathbf{Q}\cdot\hat{\mathbf{s}} + \frac{\lambda_{\mathrm{equ}}}{d}\sigma\left(\frac{|\nabla c|}{c}\right)\rho\,\hat{\mathbf{s}} - \chi\left(\frac{|\nabla c|}{c}\right)\sigma\left(\frac{|\nabla c|}{c}\right)s_i s_j \int e_i e_j\, \mathbf{e}\psi(\mathbf{r},\mathbf{e},t)\mathrm{d}\mathbf{e}. \tag{D2}$$

The last term in equation (D2) is part of the octupole moment which is defined as

$$O_{ijk} = \int [e_i e_j e_k - \frac{1}{d+2}(e_i\delta_{jk} + e_k\delta_{ij} + e_j\delta_{ki})]\psi(\mathbf{r},\mathbf{e},t)\mathrm{d}\mathbf{e}, \tag{D3}$$

and represents the interplay between tumble rate variation and tumble angle bias. By neglecting all moments above the first and again defining a relaxation rate $\omega = D_{\mathrm{rot}}(d-1) + (1-\overline{\Theta})\lambda_{\mathrm{equ}}$ we arrive at

$$\frac{\partial \mathbf{P}}{\partial t} = -\omega\mathbf{P} + D\nabla^2\mathbf{P} - \frac{v_0}{d}\nabla\rho + \frac{1-\bar{\Theta}_0}{d}\chi\left(\frac{|\nabla c|}{c}\right)\rho\frac{\nabla c}{|\nabla c|} + \frac{\lambda_{\mathrm{equ}}}{d}\sigma\left(\frac{|\nabla c|}{c}\right)\rho\frac{\nabla c}{|\nabla c|} - \left[\frac{2}{d+2}\chi\left(\frac{|\nabla c|}{c}\right)\sigma\left(\frac{|\nabla c|}{c}\right)\mathbf{P}\cdot\frac{\nabla c}{|\nabla c|}\right]\frac{\nabla c}{|\nabla c|} - \frac{1}{(d+2)}\chi\left(\frac{|\nabla c|}{c}\right)\sigma\left(\frac{|\nabla c|}{c}\right)\mathbf{P}. \tag{D4}$$

Appendix E. Time dependence of the pulse speed and effect of the initial bacterial configuration

Figure E1(a) shows the time dependence of the pulse speed $v_p(t)$ for the reference pulses from figure 2(a) (Ref I) and from figure 2(b) (Ref II), respectively. The pulse speed converges to a constant value.

In figure E1(b) we investigate the effect of the initial bacterial configuration on the pulse propagation. Changing the initial distribution from an exponential to a step profile or a linear profile has no effect on the pulse speed, indeed the curves are very close. The same is true when we change the decay length to $x_0 = 5\ \mu$m and $x_0 = 500\ \mu$m. Only for $x_0 = 5000\ \mu$m, which corresponds to 5% of the system length and which is larger than the pulse width, the curve starts to look different. Probably, when one simulates for much larger time, the pulse assumes the speed of the previous cases. As the pulse speed is directly linked to the number of bacteria in the pulse, we conclude that the maximum carrying capacity is stable for reasonable variations in the initial bacterial configuration.

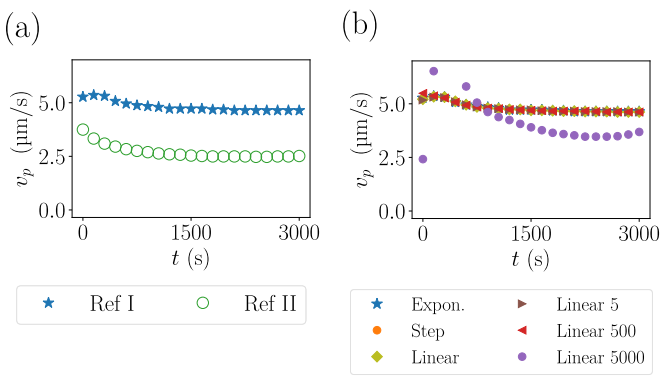

Figure E1. Pulse speed as a function of time: (a) for the reference pulse from figure 2(a); (b) for different initial configurations for the bacterial configuration. Instead of an exponential profile with decay length $x_0 = 50\ \mu$m, we try a step profile and a linear profile with the same decay length. Moreover, we also vary the decay length for the linear profile to $x_0 = \{5, 500, 5000\}\ \mu$m.

ORCID iDs

Maximilian Seyrich https://orcid.org/0000-0002-8423-2276
Holger Stark https://orcid.org/0000-0002-6388-5390

References

[1] Ramaswamy S 2010 *Annu. Rev. Condens. Matter Phys.* **1** 323
[2] Romanczuk P, Bär M, Ebeling W, Lindner B and Schimansky-Geier L 2012 *Eur. Phys. J. Spec. Top.* **202** 1
[3] Marchetti M C, Joanny J F, Ramaswamy S, Liverpool T B, Prost J, Rao M and Simha R A 2013 *Rev. Mod. Phys.* **85** 1143
[4] Zöttl A and Stark H 2016 *J. Phys.: Condens. Matter* **28** 253001
[5] Bechinger C, Di Leonardo R, Löwen H, Reichhardt C, Volpe G and Volpe G 2016 *Rev. Mod. Phys.* **88** 045006
[6] Adler J 1966 *Science* **153** 708
[7] Budrene E O and Berg H C 1991 *Nature* **349** 630
[8] Mittal N, Budrene E O, Brenner M P and Van Oudenaarden A 2003 *Proc. Natl Acad. Sci.* **100** 13259
[9] Sokolov A, Aranson I S, Kessler J O and Goldstein R E 2007 *Phys. Rev. Lett.* **98** 158102
[10] Tailleur J and Cates M 2008 *Phys. Rev. Lett.* **100** 218103
[11] Zhang H-P, Be'er A, Florin E-L and Swinney H L 2010 *Proc. Natl Acad. Sci.* **107** 13626
[12] Dombrowski C, Cisneros L, Chatkaew S, Goldstein R E and Kessler J O 2004 *Phys. Rev. Lett.* **93** 098103
[13] Reinken H, Klapp S H, Bär M and Heidenreich S 2018 *Phys. Rev.* E **97** 022613
[14] Rothschild L 1948 *J. Exp. Biol.* **25** 219
[15] Bonner J T and Savage L 1947 *J. Exp. Zoöl* **106** 1
[16] Palsson E and Othmer H G 2000 *Proc. Natl Acad. Sci.* **97** 10448
[17] Ben-Jacob E, Cohen I and Levine H 2000 *Adv. Phys.* **49** 395
[18] Strassmann J E, Zhu Y and Queller D C 2000 *Nature* **408** 965
[19] Kaiser D 2003 *Nat. Rev. Microbiol.* **1** 45
[20] Riedel I H, Kruse K and Howard J 2005 *Science* **309** 300
[21] Friedl P and Gilmour D 2009 *Nat. Rev. Mol. Cell Biol.* **10** 445
[22] Schoeller S F and Keaveny E E 2018 *J. R. Soc. Interface* **15** 20170834
[23] Saintillan D and Shelley M J 2008 *Phys. Rev. Lett.* **100** 178103
[24] Theurkauff I, Cottin-Bizonne C, Palacci J, Ybert C and Bocquet L 2012 *Phys. Rev. Lett.* **108** 268303
[25] Buttinoni I, Bialké J, Kümmel F, Löwen H, Bechinger C and Speck T 2013 *Phys. Rev. Lett.* **110** 238301
[26] Zöttl A and Stark H 2014 *Phys. Rev. Lett.* **112** 118101
[27] Pohl O and Stark H 2014 *Phys. Rev. Lett.* **112** 238303
[28] Speck T, Bialké J, Menzel A M and Löwen H 2014 *Phys. Rev. Lett.* **112** 218304
[29] Liebchen B, Marenduzzo D, Pagonabarraga I and Cates M E 2015 *Phys. Rev. Lett.* **115** 258301
[30] Pohl O and Stark H 2015 *Eur. Phys. J.* E **38** 93
[31] Blaschke J, Maurer M, Menon K, Zöttl A and Stark H 2016 *Soft. Matter* **12** 9821
[32] Kuhr J-T, Blaschke J, Rühle F and Stark H 2017 *Soft. Matter* **13** 7548
[33] Berg H C and Brown D A 1972 *Nature* **239** 500
[34] Block S M, Segall J E and Berg H C 1982 *Cell* **31** 215
[35] Berg H C 2008 *E. coli in Motion* (New York: Springer)
[36] Saragosti J, Calvez V, Bournaveas N, Perthame B, Buguin A and Silberzan P 2011 *Proc. Natl Acad. Sci.* **108** 16235
[37] Sourjik V and Wingreen N S 2012 *Curr. Opin. Cell Biol.* **24** 262
[38] Masson J-B, Voisinne G, Wong-Ng J, Celani A and Vergassola M 2012 *Proc. Natl Acad. Sci.* **109** 1802
[39] Pohl O, Hintsche M, Alirezaeizanjani Z, Seyrich M, Beta C and Stark H 2017 *PLoS Comput. Biol.* **13** e1005329
[40] Seyrich M G A, Alirezai Z, Beta C and Stark H 2018 *New J. Phys.* **20** 103033
[41] Saragosti J, Silberzan P and Buguin A 2012 *PLoS One* **7** e35412
[42] Macnab R M and Koshland D 1972 *Proc. Natl Acad. Sci.* **69** 2509
[43] De Gennes P-G 2004 *Eur. Biophys. J.* **33** 691
[44] Eisenbach M 2004 *Chemotaxis* (London: Imperial College Press)
[45] Dahlquist F, Lovely P and JUN D K 1972 *Nat. New. Biol.* **236** 120
[46] Kalinin Y V, Jiang L, Tu Y and Wu M 2009 *Biophys. J.* **96** 2439
[47] Lazova M D, Ahmed T, Bellomo D, Stocker R and Shimizu T S 2011 *Proc. Natl Acad. Sci.* **108** 13870
[48] Weber E H 1834 De pulsu, resorptione, auditu et tactu: Annotationes anatomicae et physiologicae, auctore prostat apud CF Koehler)
[49] Fechner G T 1860 Vol 2 Breitkopf und Haertel
[50] Fu X, Kato S, Long J, Mattingly H H, He C, Vural D C, Zucker S W and Emonet T 2018 *Nat. Commun.* **9** 2177
[51] Keller E F and Segel L A 1971 *J. Theor. Biol.* **30** 235
[52] Keller E F and Segel L A 1970 *J. Theor. Biol.* **26** 399
[53] Nagai T and Ikeda T 1991 *J. Math. Biol.* **30** 169
[54] Brenner M P, Levitov L S and Budrene E O 1998 *Biophys. J.* **74** 1677
[55] Othmer H G, Dunbar S R and Alt W 1988 *J. Math. Biol.* **26** 263
[56] Emako C, Gayrard C, Buguin A, de Almeida L N and Vauchelet N 2016 *PLoS Comput. Biol.* **12** e1004843
[57] Tindall M J, Maini P K, Porter S L and Armitage J P 2008 *Bull. Math. Biol.* **70** 1570
[58] Rein M, Heinß N, Schmid F and Speck T 2016 *Phys. Rev. Lett.* **116** 058102
[59] Golestanian R 2012 *Phys. Rev. Lett.* **108** 038303
[60] Stark H 2016 *Eur. Phys. J. Spec. Top.* **225** 2369
[61] Schnitzer M J 1993 *Phys. Rev.* E **48** 2553
[62] Segall J E, Block S M and Berg H C 1986 *Proc. Natl Acad. Sci.* **83** 8987
[63] Locsei J T 2007 *J. Math. Biol.* **55** 41
[64] Adler J 1969 *Science* **166** 1588

[65] Mesibov R, Ordal G W and Adler J 1973 *J. Gen. Physiol.* **62** 203
[66] Scribner T L, Segel L A and Rogers E H 1974 *J. Theor. Biol.* **46** 189
[67] Novick-Cohen A and Segel L 1984 *J. Math. Biol.* **19** 125
[68] Lapidus I R and Schiller R 1976 *Biophys. J.* **16** 779
[69] Ford R M and Lauffenburger D A 1991 *Biotechnol. Bioeng.* **37** 661
[70] Alt W 1980 *J. Math. Biol.* **9** 147
[71] Saragosti J, Calvez V, Bournaveas N, Buguin A, Silberzan P and Perthame B 2010 *PLoS Comput. Biol.* **6** e1000890
[72] Enculescu M and Stark H 2011 *Phys. Rev. Lett.* **107** 058301
[73] Cates M and Tailleur J 2013 *Europhys. Lett.* **101** 20010
[74] Press W H, Teukolsky S A, Vetterling W T and Flannery B P 2007 *Numerical Recipes 3rd Edition: The Art of Scientific Computing* (Cambridge: Cambridge University Press)
[75] Rosen G 1974 *Math. Biosci.* **20** 185
[76] Rosen G and Baloga S 1975 *Math. Biosci.* **24** 273
[77] Holz M and Chen S-H 1979 *Biophys. J.* **26** 243
[78] Rosen G 1975 *J. Theor. Biol.* **49** 311
[79] Blakemore R 1975 *Science* **190** 377
[80] Faivre D and Schuler D 2008 *Chem. Rev.* **108** 4875
[81] Young K D 2007 *Curr. Opin. Microbiol.* **10** 596
[82] Desai N, Dabiri S and Ardekani A M 2018 *Int. J. Multiph. Flow.* **108** 156
[83] Adler J 1966 *J. Bacteriol.* **92** 121
[84] Barbara G M and Mitchell J G 2003 *FEMS Microbiol. Ecol.* **44** 79
[85] Garren M, Son K, Raina J-B, Rusconi R, Menolascina F, Shapiro O H, Tout J, Bourne D G, Seymour J R and Stocker R 2014 *ISME J.* **8** 999
[86] Son K, Menolascina F and Stocker R 2016 *Proc. Natl Acad. Sci.* **113** 8624
[87] Wong-Ng J, Melbinger A, Celani A and Vergassola M 2016 *PLoS Comput. Biol.* **12** e1004974
[88] Wang P and Chen S 1986 *Biophys. J.* **49** 1205
[89] Lovely P S and Dahlquist F 1975 *J. Theor. Biol.* **50** 477